Wind and Structures, *Vol. 29, No. 1 (2019) 1-13*
DOI: https://doi.org/10.12989/was.2019.29.1.001

Forces and flow around three side-by-side square cylinders

Qinmin Zheng[1a], Md. Mahbub Alam[*1], S. Rehman[2b] and D.K. Maiti[3c]

[1]*Institute for Turbulence-Noise-Vibration Interaction and Control, Harbin Institute of Technology, Shenzhen, China*
[2]*Center for Engineering Research, Research Institute, King Fahd University of Petroleum and Minerals, Dhahran 31261, Saudi Arabia*
[3]*Department of Applied Mathematics with Oceanology and Computer Programming Vidyasagar University, Midnapur-721102, WB, India*

(Received September 7, 2018, Revised February 26, 2019, Accepted February 28, 2019)

Abstract. A numerical investigation on forces and flow around three square cylinders in side-by-side arrangement is conducted at a Reynolds number Re = 150 with the cylinder center-to-center spacing ratio L/W = 1.1 ~ 9.0, where W is the cylinder side width. The flow at this Re is assumed to be two-dimensional, incompressible, and Newtonian. The flow simulation is conducted by using ANSYS-Fluent. The flow around the three side-by-side cylinders entails some novel flow physics, involving the interaction between the gap and free-stream side flows as well as that between the two gap flows. An increase in L/W from 1.1 to 9.0 leads to five distinct flow regimes, viz., base-bleed flow (L/W < 1.4), flip-flopping flow (1.4 < L/W < 2.1), symmetrically biased beat flow (2.1 < L/W < 2.6), non-biased beat flow (2.6 < L/W < 7.25) and weak interaction flow (7.25 < L/W < 9.0). The gap flow behaviors, time-averaged and fluctuating fluid forces, time-averaged pressure, recirculation bubble, formation length, and wake width in each flow regime are discussed in detail.

Keywords: flow; forces; wake; three cylinders; gap flow

1. Introduction

The flow around cylinders has been widely investigated due to its practical significance in engineering and scientific relevance in fluid dynamics. Slender structures in mechanical, civil and naval engineering are frequently arranged in groups, for example, high-rise buildings, chimney stacks, tube bundles in heat exchangers, and bridge piers, etc. The flow around clustered cylinders, bringing in various important physical phenomena, is much more complicated than that around a single square or circular cylinder (Kang 2003, Baranyi 2003, Kumar *et al*. 2008, Sumner 2010, Kim and Alam 2015, Zhou and Alam 2016, Alam *et al*. 2017). The side-by-side arrangement is one of the most common configurations for the closely spaced structures.

Sumner *et al*. (1999) studied the flow field around two side-by-side circular cylinders subjected to a cross-flow for cylinder center-to-center spacing ratio L/D = 1.0 ~ 6.0 at Reynolds number Re = 500 ~ 3000, where Re is based on the cylinder diameter D and freestream flow velocity U_∞. Three basic vortex shedding patterns were confirmed, namely single bluff-body vortex shedding at small L/D, biased vortex shedding at intermediate L/D, and synchronized vortex shedding at larger L/D. Alam *et al.* (2003) experimentally investigated the aerodynamic characteristics of two side-by-side circular cylinders for L/D = 1.1 ~ 6.0 at Re = 5.5 × 10^4. They focused on fluctuating forces, wake frequencies, and gap-flow switching phenomena. They pioneered the measurement of fluctuating forces for two side-by-side cylinders. In addition, they for the first time identified a tristable flow, using wavelet analysis. Alam and Zhou (2007) further marked out a quadristable flow at 1.1 < L/D < 1.2. Carini *et al*. (2014) numerically investigated the origin of the flip-flopping instability occurring in the flow past two side-by-side circular cylinders at L/D = 1.6 ~ 2.4 and Re = 50 ~ 90. Their simulation results rendered new evidence that the flip-flopping state results from an instability of inphase synchronized vortex shedding between the two cylinders.

Different from the circular cylinder, the square cylinder characterized by a fixed flow separation point is a representative model of the bluff bodies with sharp corners. Alam *et al.* (2011) for two square cylinders in side-by-side arrangement performed systematic measurements of the flow field, Strouhal number, and time-averaged and fluctuating forces for center-to-center spacing ratio L/W = 1.02 ~ 6.00 and Reynolds number Re = 4.7 × 10^4, where W is the cylinder side width. With change in L/W, they observed four different flow regimes: single-body regime (1.0 < L/W < 1.3), two-frequency regime (1.3 < L/W < 2.2), transition regime (2.2 < L/W < 3.0), and coupled-vortex -street regime (L/W > 3.0). Connections were made between fluid forces and different flow regimes. Alam and Zhou (2013) conducted experiments for two side-by-side cylinders at a low Re = 300. Similarly to the experiment at Re = 4.7 × 10^4 by Alam *et al.* (2011), four flow regimes are identified at Re = 300, but L/W ranges of the four flow regimes are different from those at Re = 4.7 × 10^4. At Re = 300, single-body, two-frequency, transition, coupled-vortex -street regimes appear at 1.0 < L/W < 1.2, 1.2 < L/W < 2.1, 2.1 < L/W < 2.4, and L/W > 2.4, respectively. The switch of the gap flow was found to occur at two distinct time scales,

[*]Corresponding author, Ph.D., Professor
E-mail: alamm28@yahoo.com; alam@hit.edu.cn
[a] Ph.D.
[b] Ph.D., Professor,
[c] Ph.D., Professor

ISSN: 1226-6116 (Print), 1598-6225 (Online)

referred to as macro and micro switches. Appearing at $1.2 < L/W < 2.1$, the macro switch is characterized by the slim gap flow biased for a long duration ranging from several vortex shedding periods in the wide street to several hours. On the other hand, micro switch occurring at $2.1 < L/W < 2.4$ is characterized by the thick gap flow switching at a frequency of twice the frequency of the vortex shedding from the freestream side of the cylinders. A Floquet stability analysis was conducted by Choi and Yang (2013) to investigate the onset of three-dimensional instabilities of the flow past two side-by-side square cylinders. Six distinct Floquet modes (four A-type 3*D* modes: SA1-SA4; two B-type 3*D* modes: SB3 and SB4) were identified, and the spatial and temporal features of each mode were described in detail. For a small gap ($L/W \leq 1.3$), the flow past the two cylinders is similar to that past a single cylinder, and the critical *Re* becomes low due to the approximately doubled characteristic length. In the range of $1.6 \leq L/W \leq 1.9$, a strong wake-interference results in a drastic increase in the effective characteristic length and a quite lower critical *Re*. The interaction between the two wakes diminishes with increasing *L/W*. They also found the coexisting 3*D* instabilities for a specific base-flow topology for $2.5 \leq L/W \leq 11.0$.

Not much attention has been paid to investigations on more than two square cylinders. Based on the lattice-Boltzmann method, Kumar *et al*. (2008) investigated the flow past a row of nine square cylinders at $Re = 80$ with $L/W = 1.3 \sim 13.0$. No significant interaction between the wakes is observed for $L/W > 7.0$. At smaller *L/W*, the interaction of the wakes results in four distinct flow regimes, viz., synchronized flow ($5.0 < L/W \leq 7.0$), quasi-periodic flow-I ($4.0 \leq L/W \leq 5.0$), quasi-periodic flow-II ($2.0 < L/W < 4.0$) and chaotic flow ($L/W \leq 2.0$). A secondary frequency in addition to the primary frequency is observed in the quasi-periodic flow-I and quasi-periodic flow-II, that is supposed to be related to the transition between narrow and wide wakes behind a cylinder. The energy at the secondary frequency is contingent on *L/W*. Sewatkar *et al*. (2009) numerically investigated the flow around a row of square cylinders for $30 \leq Re \leq 140$ and $2.0 \leq L/W \leq 5.0$, focusing on the *Re* effect on steady-unsteady transition and the development of the secondary frequency. They found that the critical *Re* for the onset of vortex shedding increases with the increase of *L/W*. At a larger *L/W* (> 5.0), the continuous jet forming between two adjoining cylinders penetrates the flow domain. At a relatively small *L/W*, the lateral movement of jets closes the upstream gaps. The process of the gap closing occurs periodically with time period related to the secondary frequency in quasi-periodic flow-I and aperiodically in quasi-periodic flow-II. In the case of the chaotic flow, the lateral spread of jets is so violent that quite a few of the jets merge together.

While one-gap flow plays a role in the wake of two side-by-side cylinders, two-gap flow appears for three side-by-side cylinders where the interaction is possible between gap and freestream side flows, as well as that between two gap flows. Zheng and Alam (2017) conducted a detailed investigation on the flow around three side-by -side square cylinders for $L/W = 1.1 \sim 9.0$ and $Re = 150$. They identified five distinct flow regimes, namely base-bleed ($L/W < 1.4$), flip-flopping ($1.4 < L/W < 2.1$), symmetrically biased beat ($2.1 < L/W < 2.6$), non-biased beat ($2.6 < L/W < 7.25$) and weak interaction ($7.25 < L/W < 9.0$) flows. The fluid dynamics for three cylinders is found to be significantly different from that for two cylinders. The interaction between the two gap flows leads to a secondary frequency different from the primary frequency of vortex shedding. The physics and origin of the secondary frequency are meticulously imparted. However, some important aspects of the wake have not been paid attention to, for instance, the variation in the formation length ($L_f^* = L_f/W$), wake width ($w^* = w/W$), recirculation region, time-averaged and fluctuating fluid forces and connection between forces and L_f^* or w^*. The objective of the present study is (i) to examine the time-averaged drag ($\overline{C}_D$), time-averaged lift ($\overline{C}_L$), fluctuating (r.m.s.) drag (C'_D), fluctuating lift (C'_L), and wake size, (ii) to bridge the gap between the fluid forces and the flow regimes or gap characteristics, and (iii) to link forces with L_f^* and w^*.

2. Computational details and validation

2.1 Governing equations, numerical method and boundary conditions

The flow around three side-by-side square cylinders is simulated by solving the two-dimensional Navier-Stokes and continuity equations for an incompressible Newtonian fluid. The equations can be written in vector form in the Cartesian coordinate system as

$$\left.\begin{aligned} \frac{\partial \boldsymbol{u}^*}{\partial t^*} + \boldsymbol{u}^* \cdot \nabla \boldsymbol{u}^* &= -\nabla p^* + \frac{1}{Re}\nabla^2 \boldsymbol{u}^* \\ \nabla \cdot \boldsymbol{u}^* &= 0 \end{aligned}\right\} \quad (1)$$

where $\boldsymbol{u}^* (= \boldsymbol{u}/U_\infty)$ is the non-dimensional flow velocity vector, $p^* (= p/\rho U_\infty^2)$ is the non-dimensional pressure, t^* $(= U_\infty t/W)$ is the non-dimensional time, *Re* $(= U_\infty W/\upsilon) = 150$ is the Reynolds number. The U_∞, *W*, ρ, and υ are the freestream velocity, cylinder width, fluid density, and fluid kinematic viscosity, respectively. A commercial code, ANSYS-Fluent, was employed for the simulations. The pressure-velocity coupling is done using PISO method. The convective terms are discretized through a second-order accurate upwind differencing scheme, while the temporal discretization is handled with the second-order implicit forward discretization.

The computational domain, boundary conditions, and structured quadrangular grid distribution around the cylinders are illustrated in Figs. 1(a) and 1(b). The origin of the coordinate system is at the middle cylinder center, with the *x*- and *y*-axis being in the streamwise and lateral directions, respectively. L_u and L_d are the upstream and downstream boundary separations from the coordinate origin. The distance between the lateral boundaries is defined by L_t. The *x* and *y* are scaled with *W*, i.e., $x^* = x/W$

Table 1 Effect of mesh resolution on output and comparison of the present results with those from the literature for a single isolated cylinder with Re = 150

Sources		Elements	St	$\overline{C}_D$	C'_D	C'_L
Present	M124k (Λt^* = 0.0097)	124300	0.158	1.483	0.017	0.277
	M243k (Λt^* = 0.0048)	243256	0.159	1.474	0.016	0.270
	M450k (Λt^* = 0.0024)	450964	0.159	1.476	0.016	0.273
Kumar *et al*. (2008)		--	0.158	1.530	--	--
Sharma and Eswaran (2004)		--	0.159	1.467	--	0.291
Saha *et al*. (2003)		--	--	--	0.017	0.274
Sohankar *et al*. (1999)		--	0.165	1.440	--	0.230

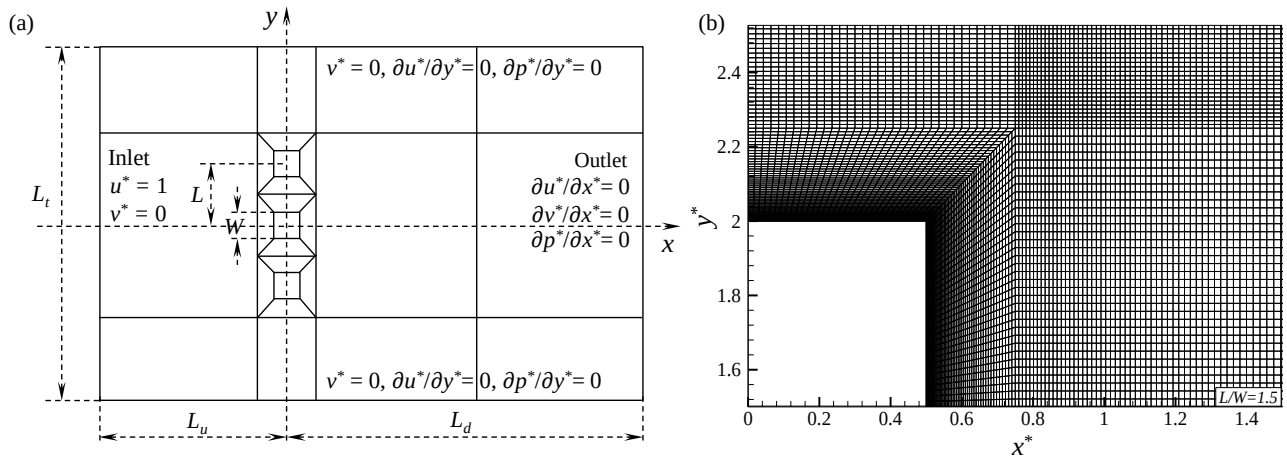

Fig. 1 (a) Sketch of the computational domain and boundary conditions, and (b) structured quadrangular grid distribution around a quadrant of a cylinder

and $y^* = y/W$. A uniform velocity profile is given at the inlet, while zero normal derivatives of the velocity components and pressure are specified at the outlet. The two lateral boundaries are given symmetry boundary conditions while the cylinder surfaces are given no-slip boundary conditions. The initial values (at $t^* = 0$) for the computational domain are set as $u^* = 1.0$, $v^* = 0$, and $p^* = 0$.

2.2 Validation of method and convergence of results

Before conducting extensive simulation for three cylinders, the grid independence test for the flow around a single cylinder was done. As presented in Table 1, three different mesh systems (M124k, M243k and M450k) are employed to study the effect of mesh resolution on the output, with the non-dimensional time step Λt^* ($= U_\infty \Delta t / W$) varying as 0.0097, 0.0048 and 0.0024, respectively. A small grid spacing of $0.0033W$ is given between the first level of the grid and cylinder wall for an adequate resolution of the boundary layer, with the grid spacing increasing with an expansion rate of 1.029 in the normal direction. The other parameters for the computation are L_u/W = 13.5, L_d/W = 29.5 and blockage ratio (BR) = W/L_t = 5.26%. Table 1 compares the Strouhal number (St = f_sW/U_∞, where f_s is the vortex shedding frequency), $\overline{C}_D$, C'_D, and C'_L for the three mesh systems. The estimations of the fluid forces include both pressure and friction components. The largest deviation among the three mesh systems (M124k, M243k and M450k) is about 2.45% for C'_L between M124k and M243k. A comparison of the present results with those from the literature for a single isolated square cylinder is illustrated in Table 1. Overall, all the integral parameters (St, $\overline{C}_D$, C'_D, and C'_L) display a good agreement with those in the literature. More details about the effect of lateral and streamwise locations of the computational boundaries on results can be found in Zheng and Alam (2017). The simulation for three side-by-side cylinders is thus given a similar mesh resolution and computational domain, i.e., $\Delta t^* = 0.0097$, $L_u/(3W) = 13.5$, $L_d/(3W) = 29.5$ and $BR = 3W/L_t = 5.26\%$.

3. Gap flow behaviors and its effect on flow field

An examination of flow structures, gap flow behaviors, and fluid forces leads to the identification of five distinct flow structures depending on L/W. They are base-bleed flow at $L/W < 1.4$, flip-flopping flow at $1.4 < L/W < 2.1$, symmetrically biased beat flow at $2.1 < L/W < 2.6$, non-

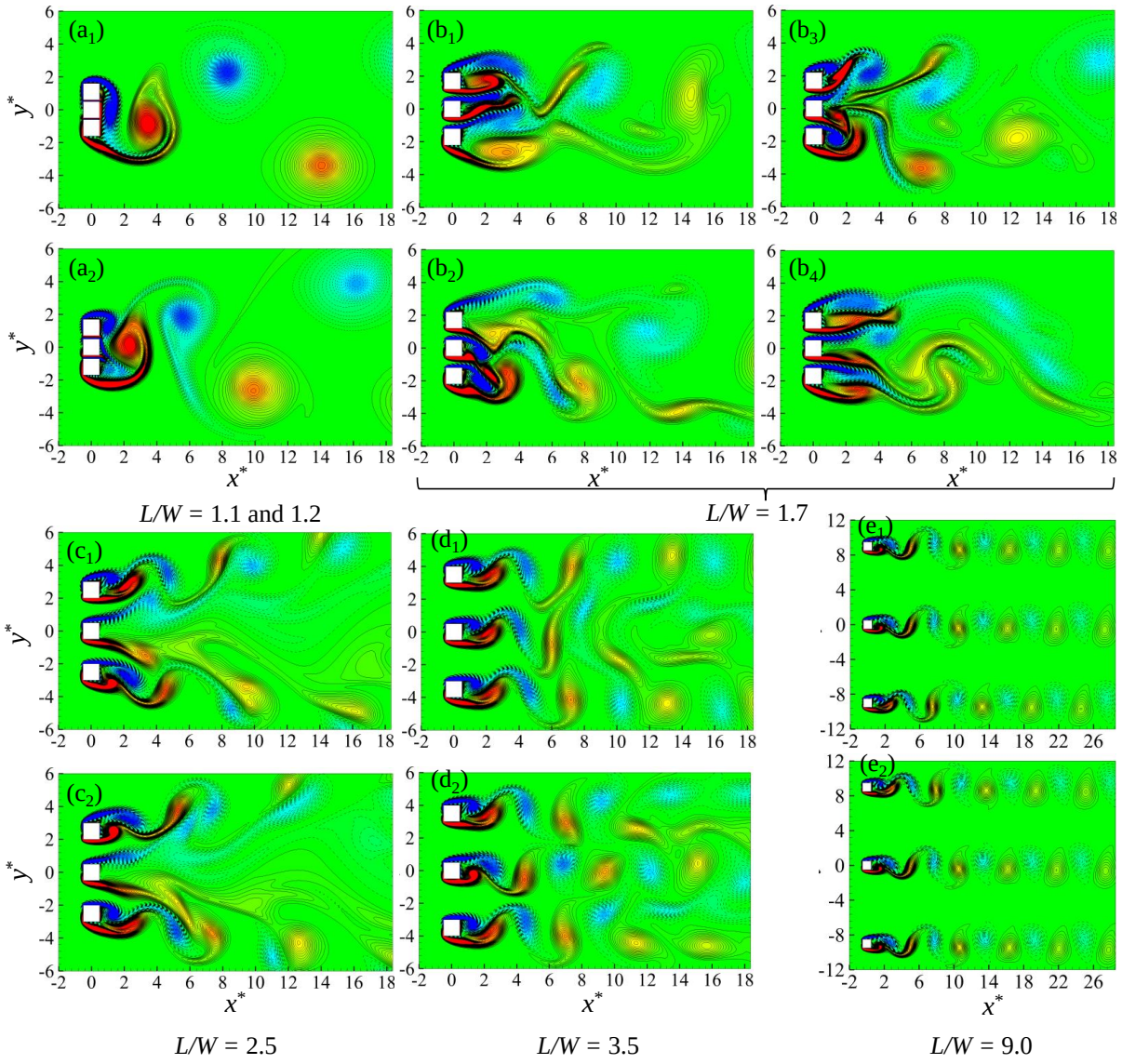

Fig. 2 Typical flow structures at different flow regimes. (a_1, a_2) base-bleed flow ($L/W < 1.4$), (b_1-b_4) flip-flopping flow ($1.4 < L/W < 2.1$), (c_1, c_2) symmetrically-biased beat flow ($2.1 < L/W < 2.6$), (d_1, d_2) non-biased beat flow ($2.6 < L/W < 7.25$); and (e_1, e_2) weak interaction flow ($7.25 < L/W < 9.0$)

biased beat flow at $2.6 < L/W < 7.25$, and weak interaction flow at $7.25 < L/W < 9.0$ (Zheng and Alam 2017).

3.1 Gap flow behaviors

Fig. 2 presents the instantaneous vorticity contours showing the gap flow behaviors for different flow regimes. Base-bleed flow is characterized by vortex shedding only from the freestream sides of the outer cylinders, forming a single Kármán vortex street behind the cylinders (Figs. 2(a_1) and 2(a_2)). As L/W is small, the flows through gaps are restricted by the cylinder-wall shear stress, being weak (L/W = 1.1, Fig. 2(a_1)) or considerable (L/W = 1.2, Fig. 2(a_2)). The flows at $L/W \leq 1.1$ and $1.1 < L/W < 1.4$ can thus be treated as weak base-bleed and strong base-bleed flows. In the flip-flopping flow, two opposite sign vortices are shed from each gap, which results in the formation of three small wakes immediately behind the cylinders. The three wakes shortly transmute into one, with the vortices from the gap flows decaying, merging and pairing with the freestream side vortices. A random switch of the gap flows from one side to the other takes place where the gap flow is biased upward, downward, outward, and straight (Figs. 2(b_1) – 2(b_4)).

In the symmetrically biased beat flow, the two gap flows deflect outward symmetrically. The two vortices from a gap interact with each other and also with the vortex from the respective freestream side. The interaction results in vortex integration and coupling between the gap flow and freestream side vortices. In this regime, the two shear layers of the middle cylinder spawn vortices almost symmetrically, not alternately, in the upper and lower wakes (Figs. 2(c_1) and 2(c_2)). In the non-biased beat flow, the gap flows are not biased anymore; the wake of each cylinder is thus

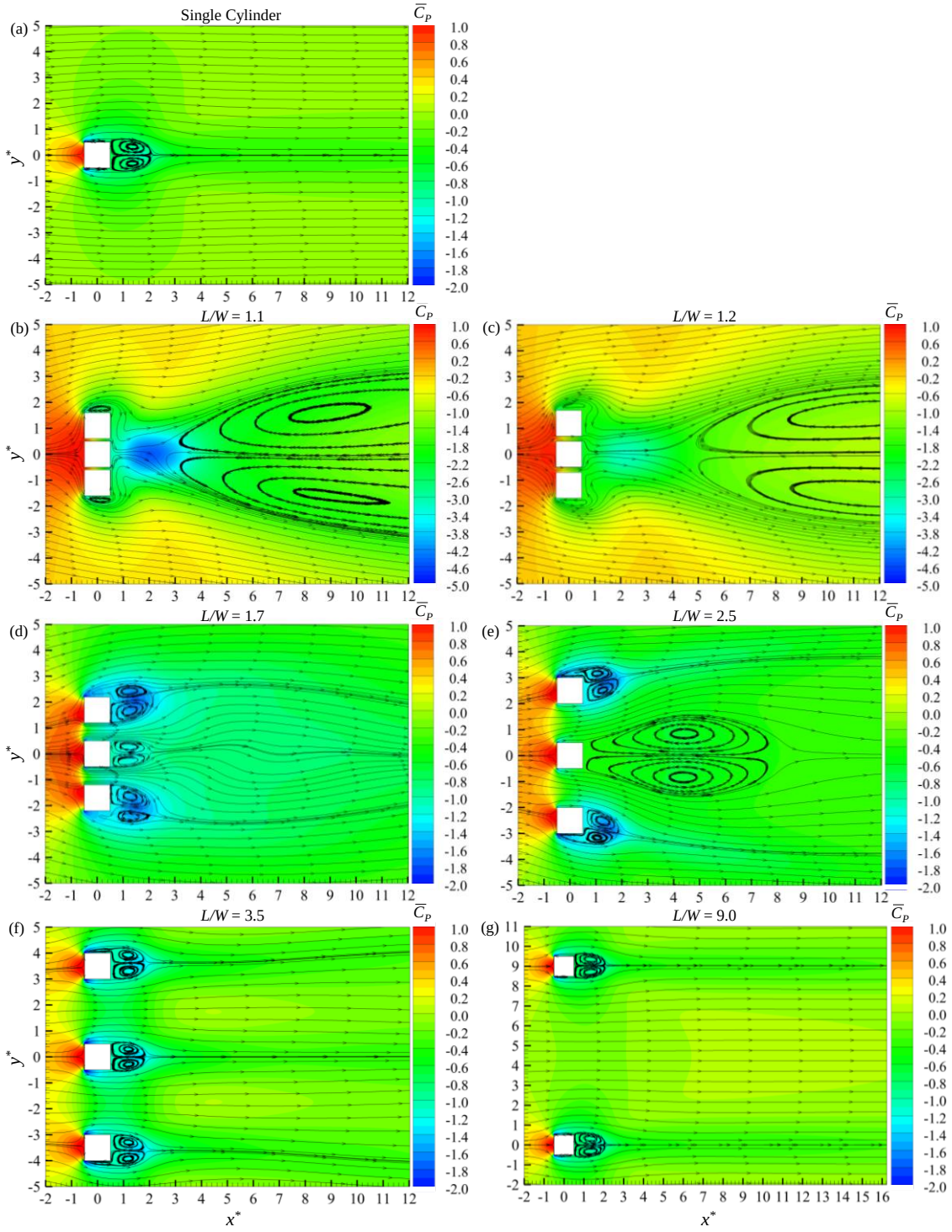

Fig. 3 Time-averaged pressure contours and streamlines. (a) Single Cylinder, (b) L/W = 1.1 (weak base-bleed flow), (c) L/W = 1.2 (strong base-bleed flow), (d) L/W = 1.7 (flip-flopping flow), (e) L/W = 2.5 (symmetrically-biased beat flow), (f) L/W = 3.5 (non-biased beat flow) and (g) L/W = 9.0 (weak interaction flow) showing only upper and middle cylinders

similar to that of an isolated cylinder. However, the interaction between vortices from the gaps leads to an irregularity of vortex arrangement and a decay of vortices particularly behind the middle cylinder (Figs. 2(d_1) and 2(d_2)). The interaction between the vortices from gaps weakens with increasing L/W, and can be ignored in the weak interaction flow (Figs. 2(e_1) and 2(e_2)).

3.2 Time-averaged pressure and streamlines

The instantaneous velocity field for an unsteady flow can be decomposed into the time-averaged and fluctuating velocity fields, e.g., $u = \overline{u} + u'$, where the 'over-bar' and 'prime' indicate time-averaged and fluctuating, respectively. The time-averaged velocity field, making a sense of steady

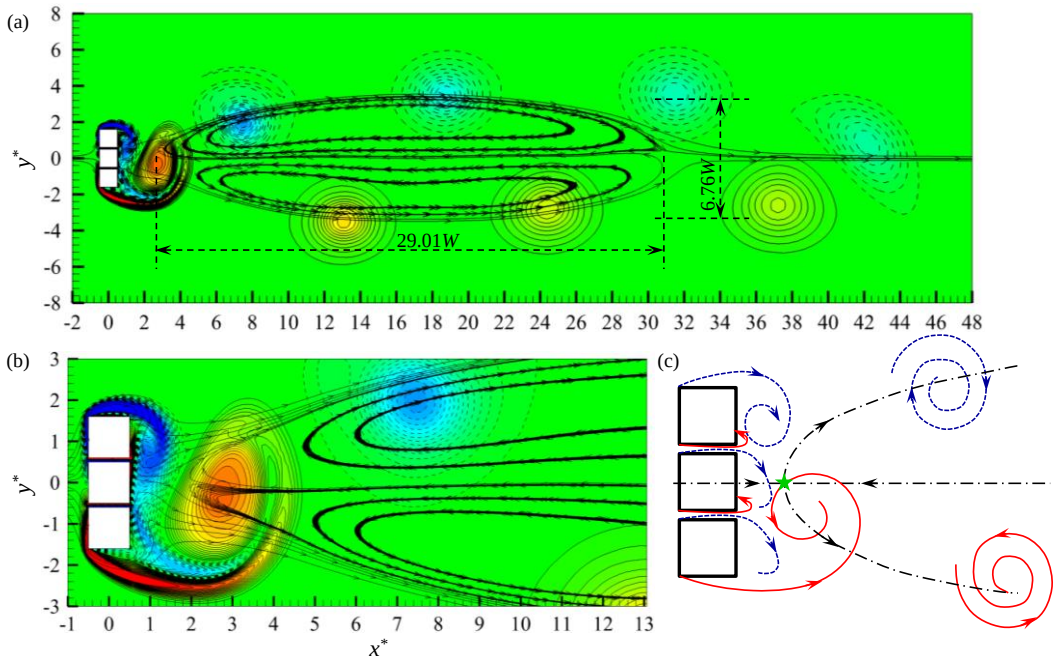

Fig. 4 (a) Instantaneous vorticity contours and recirculation bubble outline, as well as (b) their zoom-in view. (c) Sketch showing the formation of saddle point and recirculation bubble. The green star marks the position of the mean saddle point. L/W = 1.1

state, is linked with time-averaged quantities, e.g., time-averaged lift, drag, pressure, recirculation bubble, etc. The time-averaged pressure coefficient $\overline{C}_P$ contours and streamlines for the single cylinder and each flow type are illustrated in Fig. 3. As displayed in Figs. 3(b) and 3(c), $\overline{C}_P$ on the wake centerline is highly negative at $x^* \approx 2.02$ and 2.15 for L/W = 1.1 and 1.2, respectively, which is the signature of shear layer rolling. A recovery of the negative pressure occurs when L/W is increased from 1.1 to 1.2 because of greater flows through the gaps for the latter L/W (Figs. 2(a_1) and 2(a_2)). The minimum (negative) $\overline{C}_P$ behind the cylinders thus increases from -4.53 at L/W = 1.1 to -3.12 at L/W = 1.2. On the other hand, the time-averaged streamlines in Figs. 3(b) and 3(c) display a pair of large recirculation bubbles behind the three cylinders. Figure 4 displays the instantaneous vorticity contours and time-mean streamlines showing recirculation bubbles as well as their zoom-in view and sketch for L/W = 1.1. For a single cylinder, the recirculation bubbles generally appear right behind the cylinder before the saddle point, caused by the roll-up of shear layers from two sides of the cylinder (Fig. 3(a)). The recirculation bubbles for the three cylinders at L/W = 1.1 and 1.2, however, form beyond the shear-layer roll-up position. The formation mechanism of these recirculation bubbles is different from that of the bubbles occurring before the shear layer roll-up position. As will be shown later, the recirculation after the shear layer roll-up is caused by the strongly rolling convective vortices in the wake (Fig. 4(a)). While reaching the base for a single cylinder, the recirculation does not reach the base for the three-cylinder case (Figs. 3(b) and 3(c)). On the one hand, the saddle point is the boundary between the reverse and forward flows on the wake centerline. The reverse (recirculation) flow may entrap pollutants behind buildings or cause sediment accumulation behind offshore structures. On the other hand, the size of the recirculation region (saddle point position) has a close relationship with the base pressure of the cylinders, hence with the drag experienced by the cylinders.

Indeed, as illustrated in Figs. 4(b) and 4(c), the flows through the gaps confront the reverse flow and make a separatrix (saddle point, marked by the green star in Fig. 4(c)) at x^* = 2.57 and 4.53 for L/W = 1.1 and 1.2, respectively. The length and width of the recirculation bubbles are 29.01W and 6.76W, respectively, for L/W = 1.1 (Fig. 4(a)), and 16.38W and 5.26W for L/W = 1.2. The shrink of the recirculation bubble is due to the stronger gap flows (at L/W = 1.2) that postpone the shear layer roll-up position and enable a faster pinch off for the shear layers from the freestream sides of the outer cylinders. The vortices shed are thus relatively weaker and have relatively smaller lateral separation from the center line. The presence of such a pair of large recirculation bubbles at such large x^* was unexpected and identified for the first time to the authors' knowledge. Engineers should pay attention to the formation of these large recirculation bubbles that may entrap pollutants behind buildings or cause sediment accumulation or transportation behind offshore structures and bridge piers.

As presented in Fig. 3(d), a pair of recirculation bubbles persist behind each cylinder, attaching on the rear surface of the cylinders at L/W = 1.7 (flip-flopping flow). The recirculation bubbles are smaller for the middle cylinder, and the centerline of the recirculation deflects outward for the outer cylinders, due to the fact that the middle and outer

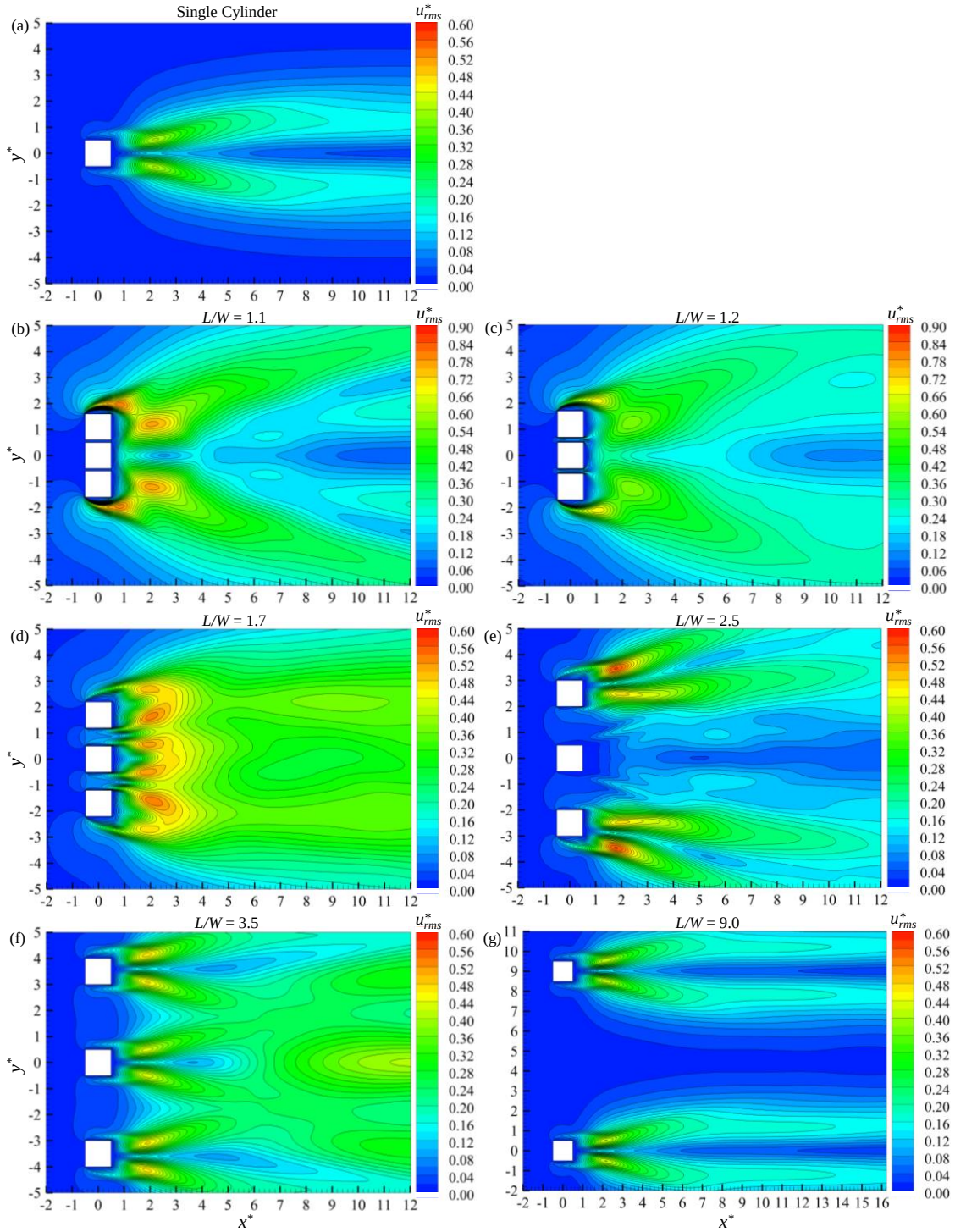

Fig. 5 The r.m.s. streamwise velocity u^*_{rms} contours. (a) Single Cylinder, (b) L/W = 1.1 (weak base-bleed flow), (c) L/W = 1.2 (strong base-bleed flow), (d) L/W = 1.7 (flip-flopping flow), (e) L/W = 2.5 (symmetrically-biased beat flow), (f) L/W = 3.5 (non-biased beat flow) and (g) L/W = 9.0 (weak interaction flow) showing only upper and middle cylinders

cylinders undergo the narrow and wide wakes most of the time, respectively (Figs. 2(b_1)-(b_4)). The negative pressure behind the middle cylinder is weaker in magnitude than that behind the outer cylinders. The minimum pressure equals to -1.24 and -1.69 behind the middle and outer cylinders, respectively.

As discussed for the symmetrically biased beat flow, the two gap flows deflect symmetrically outward, and the two shear layers of the middle cylinder spawn vortices in the upper and lower wakes almost symmetrically. A pair of large recirculation bubbles thus prevails behind the middle cylinder, the magnitude of the minimum pressure (= -0.63)

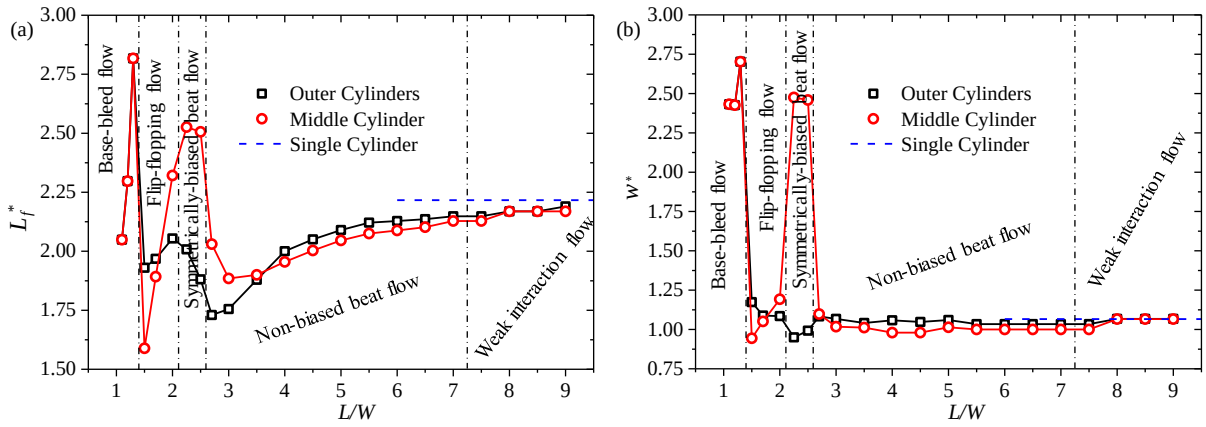

Fig. 6 Variations in (a) formation length L_f^* and (b) wake width w^* with L/W

being small (Fig. 3(e)). The length and width of the recirculation bubbles are about 8.05W and 3.14W, respectively. This is about 3.83 and 2.54 times larger than those of a single square cylinder (Fig. 3(e)). On the other hand, the outer cylinders each has recirculation bubbles close to the base, with a larger magnitude of the minimum pressure (= -1.71).

In the non-biased beat flow, the shape and size of the recirculation bubbles behind each cylinder is similar to that behind an isolated cylinder (Fig. 3(f)). The negative pressure is slightly stronger behind the outer cylinders than behind the middle cylinder, due to the interaction between the vortices from gaps behind the middle cylinder. At L/W = 3.5, the minimum pressure equals to -1.37 and -1.41 behind the middle and outer cylinders, respectively. With increasing L/W, as the interaction between the vortices from gaps weakens, the difference in recirculation bubble size or minimum negative pressure between the middle and outer cylinders gets smaller. The difference is negligible in the weak interaction flow (Fig. 3(g)).

3.3 Fluctuating streamwise velocity and wake parameters

Fig. 5 shows the root-mean-square (r.m.s.) streamwise velocity (u_{rms}^*) contours for the single cylinder and each flow type, while variations in the formation length (L_f^*) and wake width (w^*) with L/W are presented in Fig. 6. Here, L_f^* is the streamwise separation between the cylinder center and the point of maximum u_{rms}^* in the wake, and w^* refers to the transverse separation between the two maxima in the u_{rms}^* contours (Alam *et al.* 2011, Younis *et al.* 2016).

In the weak base-bleed flow (L/W = 1.1), the shear layers start to curl at the rear edge of the outer cylinders, and the vortices accumulating vorticity from the shear layer grows and recedes (Figs. 2(a_1) and 5(b)). The eventual formation of vortices occurs at x^* = 2.05 = L_f^* which is slightly smaller than the single cylinder counterpart (L_f^*= 2.22). The maximum u_{rms}^*, however, exceeds that in the single cylinder wake. In the strong base-bleed flow (L/W = 1.2), the visible gap flows interacting with the freestream-side shear layers postpone the vortex formation length and lessen the maximum u_{rms}^* value (Figs. 5(b) and 5(c)). The L_f^* = 2.30 and 2.82 for L/W = 1.2 and 1.3, respectively (Figs. 5(c) and 6(a)).

In the flip-flopping flow, the gap flows split the wake into three immediately behind the cylinders, as such there are two maximum u_{rms}^* points behind each cylinder (Fig. 5(d)). The streamwise positions of two maximum u_{rms}^* are not the same for each of the outer cylinders. For the L_f^* estimation (Fig. 6), the average of the two was considered. The wake width thus collapses from $w^* \approx 2.70$ at L/W = 1.3 to $w^* \approx 1.17$ and 0.94 for the outer and middle cylinders at L/W = 1.5 (Fig. 6(b)). With an increase in L/W, the gap flows get stronger, and become straight or deflect outward. Consequently, as presented in Figs. 6(a) and 6(b)), the wake widths for the outer and middle cylinders slightly decrease and increase, respectively, while the formation lengths for the outer and middle cylinders elongate slightly and sharply, respectively. The $L_f^* \approx 2.05$ and 2.32, $w^* \approx$ 1.08 and 1.19 for the outer and middle cylinders, respectively, at L/W = 2.0. The maximum u_{rms}^* values behind the middle cylinder are much smaller than those behind the outer cylinders for the symmetrically biased beat flow (Fig. 5(e)), and the u_{rms}^* contours behind the outer cylinders deflect outward symmetrically. In this regime, both formation length and wake width are larger for the middle cylinder than the outer cylinders. For instance, at L/W = 2.5, $L_f^* \approx 1.88$ and 2.51, $w^* \approx 0.99$ and 2.46 for outer and middle cylinders, respectively.

The gap flows do not direct outward anymore in the non-biased beat flow, and the arrangement of vortices behind each cylinder in the near wake is similar to that behind a single cylinder. An irregularity of vortex arrangement behind the middle cylinder due to the interaction between vortices from the gaps (Figs. 2(d_1) and 2(d_2)) is also manifested by the local maximum u_{rms}^* at $x^* \approx 12.30$, shown in Fig. 5(f). The w^* for the middle cylinder is slightly smaller than that for an outer cylinder (Fig. 6(b)), owing to the squeeze effect from the shear layers of outer cylinders. The difference decreases with the increasing of

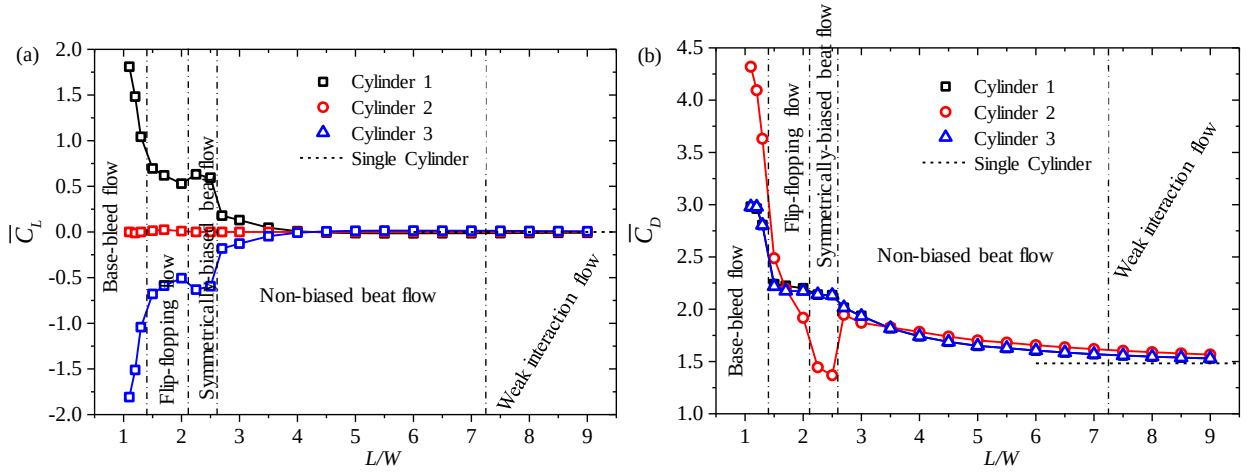

Fig. 7 Variations in time-mean (a) lift $\overline{C}_L$ and (b) drag $\overline{C}_D$ coefficients with *L/W*

L/W, vanishing in the weak interaction flow. On the other hand, L_f^* for the middle cylinder is larger than that for an outer cylinder at *L/W* = 2.6 - 3.5, but slightly smaller at 3.5 < *L/W* < 7.25. The L_f^* for the middle or outer cylinders increases with increasing *L/W* and approaches that for a single cylinder at *L/W* ≥ 8.0.

4. Time-averaged and fluctuating fluid forces

4.1 Time-averaged fluid forces

Variations in $\overline{C}_L$ and $\overline{C}_D$ with *L/W* are presented in Fig. 7. In the base-bleed flow, the vortex shedding occurs only from the freestream sides of the outer cylinders, and the gap flows between the cylinders appear weak for *L/W* ≤ 1.1 (weak base-bleed flow, Fig. 2(a_1)) and appreciable for 1.1 < *L/W* < 1.4 (strong base-bleed flow, Fig. 2(a_2)). Consequently, for an outer cylinder, the pressure is more negative on the outer side surface than on the inner. The time-averaged lift coefficients for the outer cylinders are thus repulsive. The difference in pressure between the inner and outer surfaces gets smaller with increasing *L/W* (Figs. 3(b) and 3(c)), which leads to a decreasing $\overline{C}_L$ magnitude with *L/W*; $|\overline{C}_L| \approx 1.81$ at *L/W* = 1.1, and $|\overline{C}_L| \approx 1.04$ at *L/W* = 1.3 (Fig. 7(a)). Because of the symmetry of the flow, $\overline{C}_L$ = 0 for the middle cylinder. The appreciable gap flows prolong the vortex formation and enhance the velocity recovery in the near wake. The magnitude of minimum (negative) pressure in the near wake thus wanes (Figs. 3(b) and 3(c)), and $\overline{C}_D$ declines, particularly for the middle cylinder; $\overline{C}_D \approx 4.32$ and 3.63 at *L/W* = 1.1 and 1.3, respectively (Fig. 7(b)). As *L/W* enlarges (flip-flopping flow), a greater flow can pass through the gaps and split the wake into three immediately downstream of the cylinders. The gap flows further diminish the pressure difference between the outer and inner surface of an outer cylinder. The $\overline{C}_L$ magnitudes for the outer cylinders thus further shrink with *L/W* (Fig. 7(a)). As L_f^* dramatically stretches with *L/W*, dominating the w^* increase, $\overline{C}_D$ of the middle cylinder declines distinctly ($\overline{C}_D \approx 2.49$ at *L/W* = 1.5, and $\overline{C}_D \approx 1.92$ at *L/W* = 2.0), while that of an outer cylinder also decreases, albeit a little ($\overline{C}_D \approx 2.23$ at *L/W* = 1.5, and $\overline{C}_D \approx 2.19$ at *L/W* = 2.0). In the symmetrically biased flow, a small increase in $\overline{C}_L$ magnitude of an outer cylinder is discernible, $|\overline{C}_L| \approx 0.63$ and 0.59 at *L/W* = 2.25 and 2.5, respectively (Fig. 7(a)). As discussed above, a substantially wide wake accompanies the middle cylinder, and a narrow wake complements each outer cylinder. Consequently, the base pressure magnitude for the middle cylinder is much smaller than that for the outer cylinders, which engenders a smaller $\overline{C}_D$ magnitude (≈ 1.41) for the middle cylinder (Fig. 7(b)). As the gap flows are no longer biased and a single vortex street persists behind each cylinder in the non-biased beat flow (Figs. 2(d_1) and 2(d_2)), the magnitude of $\overline{C}_L$ for the outer cylinders collapses from 0.60 (*L/W* = 2.5) to 0.18 (*L/W* = 2.7) and decreases gradually, converging towards zero (Fig. 7(a)). The magnitudes of $\overline{C}_D$ for the cylinders are close to one another, dwindling gradually with *L/W* ($|\overline{C}_D| \approx 1.99$ and 1.59 at *L/W* = 2.7 and 7.0, respectively; Fig. 7(b)), accompanied by an increasing formation length, $L_f^* \approx 1.73$ at *L/W* = 2.7 and $L_f^* \approx 2.15$ at *L/W* = 7.0. In the weak interaction flow, both $\overline{C}_L$ and $\overline{C}_D$ for all three cylinders are close to those for an isolated cylinder (Figs. 7(a) and 7(b)), as expected.

4.2 Fluctuating fluid forces

Fig. 8 presents the dependence on *L/W* of fluctuating lift and drag coefficients (C_L' and C_D') of the cylinders. In the base-bleed flow, the swerving of the outer shear layers lessens with *L/W* due to the effect of gap flows, which causes the C_L' magnitude of the outer cylinders decreasing sharply, from 1.33 at *L/W* = 1.1 to 0.63 at *L/W* = 1.3. At *L/W* = 1.2, the swerving direction of both gap-flows with small vortices follows the shedding from the freestream sides, and the gap flows are less biased at *L/W* = 1.3. The C_L'

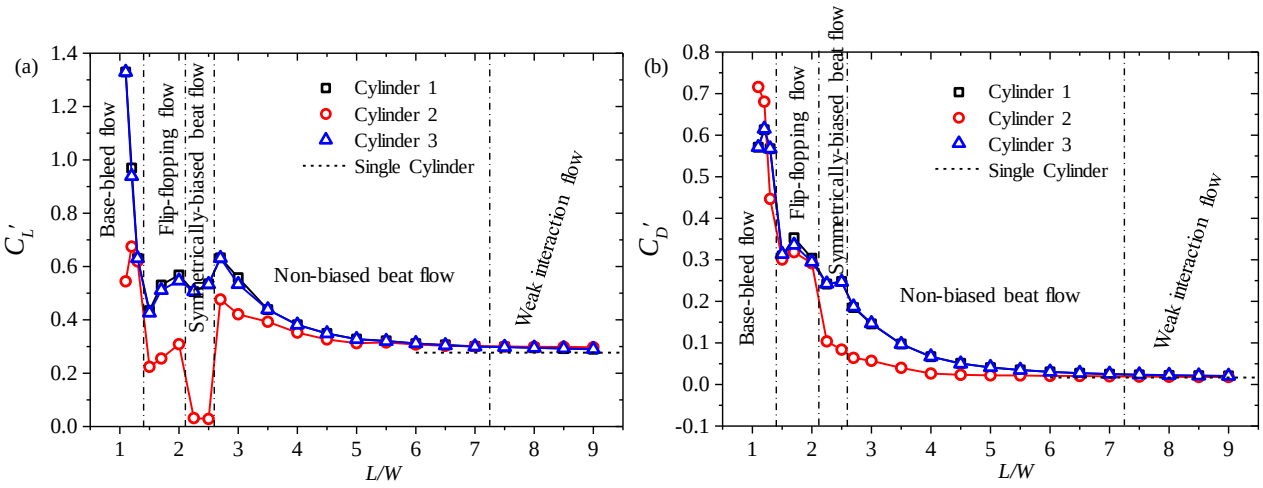

Fig. 8 Variations in fluctuating (a) lift C_L' and (b) drag C_D' coefficients with L/W

magnitude of the middle cylinder thus increases between L/W = 1.1 and 1.2 and decreases L/W = 1.2 and 1.3 ($C_L' \approx$ 0.54, 0.67 and 0.62 for the middle cylinder at L/W = 1.1, 1.2 and 1.3, respectively, Fig. 8(a)). The vortex formation occurs very close to the base of the middle cylinders at L/W = 1.1 (Fig. 2(a_1)) while moving away from the wake centerline and also from the cylinders for 1.1 < L/W < 1.4 (Fig. 6). The C_D' thus monotonically declines for the middle cylinder but has a mixed behavior for the outer cylinders (Fig. 8(b)). In the flip-flopping flow, and the C_L' is small for the middle cylinder and increases with L/W for all cylinders (Fig. 8(a)). The observation implies that the gap flows swing more frequently and/or violently. Again, C_D' has a mixed variation for all the cylinders in this regime. In the symmetrically biased beat flow, the middle cylinder experiences a lower C_L' (≈ 0.03) and C_D' (≈ 0.09) (Figs. 8(a) and 8(b)) because the two shear layers of the middle cylinder shed vortices almost symmetrically. As the flow steps from the symmetrically biased beat flow to the non-biased beat flow, the vortices from the middle cylinder sheds alternately in the wake; consequently, the C_L' of the middle and outer cylinders has a distinct jump, from $C_L' \approx$ 0.03 and 0.54 at L/W = 2.5 to $C_L' \approx$ 0.48 and 0.63 at L/W = 2.7. With increasing L/W in the non-biased beat flow and weak interaction flow, both C_L' and C_D' decline for all three cylinders and converge toward that for an isolated cylinder (Figs. 8(a) and 8(b)). The dependence of different parameters on L/W or different flow regimes can be summarized in Table 2. The additional subscripts 'O', 'M' and 'S' following the parameters in this table stand for the outer, middle and single cylinders, respectively; while the arrows '↘' and '↗' refer to decrease and increase, respectively.

5. Conclusions

A detailed study has been conducted on forces and wake structures of three side-by-side square cylinders for L/W = 1.1 ~ 9.0 and Re = 150. The flow is assumed to be two-dimensional, incompressible, and Newtonian. The ANSYS-Fluent was used to simulate the flow. The focus is given on five distinct flows including the gap flow behaviors, time-averaged pressure, recirculation bubble, formation length (L_f^*), wake width (w^*), along with time-averaged and fluctuating fluid forces ($\overline{C}_L$, C_L', $\overline{C}_D$ and C_D') on cylinders.

In the base-bleed flow (L/W < 1.4), vortices shed only from the freestream sides of the outer cylinders, forming a single Kármán vortex street. A highly negative pressure region thus persists behind the three cylinders. A pair of large recirculation bubbles prevail beyond the shear-layer roll-up position. The formation mechanism of these recirculation bubbles is different from that of classical bubbles behind a single cylinder. While the bubbles for a single cylinder form before the shear layer roll-up, those for the base-bleed flow form after the shear layer roll-up, resulting from the strong rolling of convective vortices in the wake. The length and width of the recirculation bubbles are 29.01W and 6.76W for L/W = 1.1 and 16.38W and 5.26W for L/W = 1.2. Both L_f^* and w^* enlarge with increasing L/W due to the enhanced flows through the gap. The magnitudes of $\overline{C}_L$ and C_L' for the outer cylinders are larger than those for the middle cylinder, declining rapidly with increasing L/W; while C_L' for the middle cylinder swells and shrinks at L/W < 1.2 and 1.2 ≤ L/W < 1.4, respectively. The $\overline{C}_D$ is larger for the middle cylinder than for the outer cylinders, decreasing sharply for the former cylinder and mildly for the latter cylinders with an increase in L/W. The C_D' for the middle cylinder wanes monotonously while that for the outer cylinders grows and declines in L/W < 1.2 and 1.2 ≤ L/W < 1.4, respectively.

The two-gap flow with appreciable vortices, splits the wake into three immediately behind the cylinders in the flip-flopping flow (1.4 < L/W < 2.1), and the three wakes marge into one shortly. A pair of recirculation bubbles persists behind each cylinder, attaching on its rear surface. The magnitude of the minimum pressure behind the middle

Table 2 Variations in fluid forces with *L/W* at different flow regimes

Flows	Lift	Drag
Base-bleed	$\lvert\overline{C}_{LO}\rvert\searrow > \lvert\overline{C}_{LM}\rvert \approx 0.0$ $C'_{LO}\searrow > C'_{LM}\nearrow > C'_{LS}$ ($L/W < 1.2$) $C'_{LO}\searrow > C'_{LM}\searrow > C'_{LS}$ ($L/W \geq 1.2$)	$\overline{C}_{DM}\searrow > \overline{C}_{DO}\searrow > \overline{C}_{DS}$ $C'_{DM}\searrow > C'_{DO}\nearrow > C'_{DS}$ ($L/W < 1.2$) $C'_{DM}\searrow > C'_{DS}$, $C'_{DO}\searrow > C'_{DS}$ ($L/W \geq 1.2$)
Flip-flopping	$\lvert\overline{C}_{LO}\rvert\searrow > \lvert\overline{C}_{LM}\rvert \approx 0.0$ $C'_{LO}\nearrow > C'_{LS} > C'_{LM}\nearrow$	$\overline{C}_{DO}\searrow > \overline{C}_{DS}$; $\overline{C}_{DM}\searrow > \overline{C}_{DS}$ $C'_{DO}\nearrow \approx C'_{DM}\nearrow > C'_{DS}$ ($L/W < 1.7$) $C'_{DO}\searrow \approx C'_{DM}\searrow > C'_{DS}$ ($L/W \geq 1.7$)
Symmetrically biased beat	$\lvert\overline{C}_{LO}\rvert\searrow > \lvert\overline{C}_{LM}\rvert \approx 0.0$ $C'_{LO}\nearrow > C'_{LS} > C'_{LM}\searrow$	$\overline{C}_{DO}\searrow > \overline{C}_{DS} > \overline{C}_{DM}\searrow$ $C'_{DO}\nearrow > C'_{DM}\searrow > C'_{DS}$
Non-biased beat	$\lvert\overline{C}_{LO}\rvert\searrow > \lvert\overline{C}_{LM}\rvert \approx 0.0$ $C'_{LO}\searrow > C'_{LM}\searrow > C'_{LS}$	$\overline{C}_{DO}\searrow \approx \overline{C}_{DM}\searrow > \overline{C}_{DS}$ $C'_{DO}\searrow > C'_{DM}\searrow > C'_{DS}$
Weak interaction	$\lvert\overline{C}_{LO}\rvert \approx \lvert\overline{C}_{LM}\rvert \approx 0.0$ $C'_{LO} \approx C'_{LM} \approx C'_{LS}$	$\overline{C}_{DO} \approx \overline{C}_{DM} \approx \overline{C}_{DS}$ $C'_{DO} \approx C'_{DM} \approx C'_{DS}$

cylinder is smaller than that behind the outer cylinders. The outer and middle cylinders have a decreasing and increasing w^* with *L/W*, respectively. On the other hand, L_f^* enlarges with *L/W* for all three cylinders, mildly for the outer cylinders and sharply for the middle cylinder. The $\overline{C}_L$ and $\overline{C}_D$ for the outer cylinders dwindle slightly with *L/W*, and the $\overline{C}_D$ for the middle cylinder falls sharply again. The C'_L is smaller for the middle cylinder than for the outer cylinders, increasing for all cylinders with *L/W*. The C'_D is almost the same for the three cylinders.

In the symmetrically biased beat flow ($2.1 < L/W < 2.6$), the two gap flows defect outward, and the two shear layers of the middle cylinder spawn vortices almost symmetrically in the upper and lower wakes. A pair of large and small recirculation bubbles prevail behind the middle and outer cylinders, respectively. The minimum pressure behind the middle cylinder is much smaller in magnitude than that behind the outer cylinders. Both L_f^* and w^* for the middle cylinder are larger than those for the outer cylinders. The $\overline{C}_D$, C'_L and C'_D for the middle cylinder become smaller than those for the outer cylinders.

The wake of each cylinder is similar to that of an isolated cylinder in the non-biased beat flow ($2.6 < L/W < 7.25$). However, a strong interaction between vortices from the gaps occurs, particularly behind the middle cylinder. The w^* for the middle cylinder is slightly smaller than that for the outer cylinders while the L_f^* for the middle cylinder is larger than the outer cylinder counterpart at $L/W \leq 3.5$, but slightly smaller at $3.5 < L/W < 7.25$. The L_f^* increases with *L/W* for all cylinders. The $\overline{C}_D$ magnitudes for all cylinders are close to one another and declines with *L/W*. The C'_L and C'_D for the outer cylinders exceed those for the middle cylinder, with the difference getting smaller with an increase in *L/W*. The interaction between the vortices from gaps is negligible in the weak interaction flow ($7.25 < L/W < 9.0$). All parameters approach a single cylinder counterpart.

Acknowledgments

The second author wishes to acknowledge the support given by the National Natural Science Foundation of China through Grants 11672096 and 91752112 and by Research Grant Council of Shenzhen Government through grant JCYJ20170811152808282.

References

Alam, M.M., Moriya, M. and Sakamoto, H. (2003), "Aerodynamic characteristics of two side-by-side circular cylinders and application of wavelet analysis on the switching phenomenon", *J. Fluid. Struct.*, **18**(3-4), 325-346. https://doi.org/10.1016/j.jfluidstructs.2003.07.005.

Alam, M.M. and Zhou, Y. (2013), "Intrinsic features of flow around two side-by-side square cylinders", *Phys. Fluids*, **25**(8), 085106. https://doi.org/10.1063/1.4817670.

Alam, M.M. and Zhou, Y. (2007), "Flow around two side-by-side closely spaced circular cylinders", *J. Fluid. Struct.*, **23**(5),799-805. https://doi.org/10.1016/j.jfluidstructs.2006.12.002.

Alam, M.M., Zhou, Y. and Wang, X.W. (2011), "The wake of two side-by-side square cylinders," *J. Fluid Mech.*, **669**, 432-471. https://doi.org/10.1017/S0022112010005288.

Alam, M.M., Zheng, Q. and Hourigan, K. (2017), "The wake and thrust by four side-by-side cylinders at a low Re", *J. Fluid. Struct.*, **70**, 131-144. https://doi.org/10.1016/j.jfluidstructs.2017.01.014.

Baranyi, L. (2003), "Computation of unsteady momentum and heat transfer from a fixed circular cylinder in laminar flow", *J. Comput. Appl. Mech.*, **4**(1), 13-25.

Carini, M., Giannetti, F. and Auteri, F. (2014), "On the origin of the flip–flop instability of two side-by-side cylinder wakes", *J. Fluid Mech.*, **742**, 552-576. https://doi.org/10.1017/jfm.2014.9.

Choi, C. and Yang, K. (2013), "Three-dimensional instability in the flow past two side-by-side square cylinders", *Phys. Fluids*, **25**(7), 74107. https://doi.org/10.1063/1.4813628.

Kang, S. (2003), "Characteristics of flow over two circular cylinders in a side-by-side arrangement at low Reynolds numbers", *Phys. Fluids*, **15**(9), 2486. https://doi.org/10.1063/1.1596412.

Kim, S., and Alam, M.M. (2015), "Characteristics and suppression of flow-induced vibrations of two side-by-side circular cylinders", *J. Fluid. Struct.*, **54**, 629-642. https://doi.org/10.1016/j.jfluidstructs.2015.01.004.

Kumar, S. R., Sharma, A. and Agrawal, A. (2008), "Simulation of flow around a row of square cylinders", *J. Fluid. Mech.*, **606**, 369-397. https://doi.org/10.1017/S0022112008001924.

Saha, A.K., Biswas, G. and Muralidhar, K. (2003), "Three-dimensional study of flow past a square cylinder at low Reynolds numbers", *Int. J. Heat Fluid Fl.*, **24**(1), 54-66. https://doi.org/10.1016/S0142-727X(02)00208-4.

Sewatkar, C.M., Sharma, A. and Agrawal, A. (2009), "On the effect of Reynolds number for flow around a row of square cylinders", *Phys. Fluids*, **21**(8), 083602. https://doi.org/10.1063/1.3210769.

Sharma, A. and Eswaran, V. (2004), "Heat and fluid flow across a square cylinder in the two-dimensional laminar flow regime", *Numer. Heat T. A: Appl.*, **45**(3), 247-269. https://doi.org/10.1080/10407780490278562.

Sohankar, A., Norberg, C. and Davidson, L. (1999), "Simulation of three-dimensional flow around a square cylinder at moderate Reynolds numbers", *Phys. Fluids*, **11**(2), 288-306. https://doi.org/10.1063/1.869879.

Sumner, D., Wong, S., Price, S.J. and Paidoussis, M.P. (1999), "Fluid behaviour of side-by-side circular cylinders in steady cross-flow", *J. Fluid. Struct.*, **13**(3), 309-338. https://doi.org/10.1006/jfls.1999.0205.

Sumner, D. (2010), "Two circular cylinders in cross-flow: a review", *J. Fluid. Struct.*, **26**(6), 849-899. https://doi.org/10.1016/j.jfluidstructs.2010.07.001.

Younis, M.Y., Alam, M.M. and Zhou, Y. (2016), "Flow around two non-parallel tandem cylinders", *Phys. Fluids*, **28**(12), 125106. https://doi.org/10.1063/1.4972549

Zheng, Q. and Alam, M.M. (2017), "Intrinsic features of flow past three square cylinders in side-by-side arrangement", *J. Fluid Mech.*, **826**, 996-1033. https://doi.org/10.1017/jfm.2017.378.

Zhou, Y. and Alam, M.M. (2016), "Wake of two interacting cylinders: a review", *Int. J. Heat Fluid Fl.*, **62**, 510-537.

Nomenclature

Re: Reynolds number
St: Strouhal number
L: center-to-center spacing between the cylinders
L_u: upstream boundary separation from the coordinate origin
L_d: downstream boundary separation from the coordinate origin
D: circular cylinder diameter
W: square cylinder side width
$\overline{C}_D$: time-mean drag coefficient
$\overline{C}_L$: time- mean lift coefficient
$\overline{C}_P$: time- mean pressure coefficient
C'_D: fluctuating (r.m.s.) drag coefficient
C'_L: fluctuating (r.m.s.) lift coefficient
L_f^*: normalized formation length
w^*: normalized wake width
$\boldsymbol{u}^*$: non-dimensional flow velocity vector
p^*: non-dimensional pressure
t^*: non-dimensional time
U_∞: freestream velocity
ρ: fluid density
υ: kinematic viscosity of fluid
f_s: vortex shedding frequency
u^*_{rms}: fluctuating (r.m.s.) streamwise velocity